Code Division-based Sensing of Illumination Contributions in Solid-State Lighting

Jean-Paul M. G. Linnartz, Lorenzo Feri, Hongming Yang, Sel B. Colak and Tim C. W. Schenk

Abstract

In recent years, light-emitting diode (LED) technology emerged as a prime candidate for the future illumination light source, due to high energy efficiency and long life time. In addition, LEDs offer a superior flexibility in terms of colors and shapes, which leads to a potentially infinite variety of available light patterns. In order to create these patterns via easy user interaction, we need to sense the local light contribution of each LED. This measurement can be enabled through tagging of the light of each LED with unique embedded IDs. To this end, we propose a new family of modulation and multiple access schemes in this paper and show how they can be applied to accurately estimate the local light contributions.

First we will introduce *code-time division multiple access - pulse position modulation (CTDMA-PPM)*: a form of PPM which is keyed according to a spreading sequence, and in which the duty cycle is compatible to any pulse width modulation (PWM) set by the required lighting setting. Another scheme proposed is CTDMA-PWM, where, in contrast to CTDMA-PPM, we modulate only the start position of a pulse, but not the end position. Our schemes satisfy luminary-dependent illumination constraints, in addition to the multi-signal separation requirements for simultaneous (hence CDMA) measurement of illumination strength. To our best knowledge, this combination has not been addressed previously by other optical modulation methods, which mainly aimed at high downlink throughout for a common data stream. Based on the proposed modulation methods and multiple access schemes, we develop a system structure, which includes PWM illumination sources, a sensor receiver and a control system. Performance analyses show that even for a very large number of LEDs, the sensing performance of the system satisfies the posed requirements up to an adequate range.

Index Terms

Light-emitting diodes, lighting control, code division multiple access, pulse position modulation, pulse width modulation.

I. INTRODUCTION

Light-emitting diodes (LEDs) will capture a significant portion of the market for illumination and may largely replace incandescent and gas discharge lamps in the future [2]. The progress in luminance delivered by LED technology follows an exponential trend of doubling every 18-24 months. By the time of publishing this paper, presumably commercial LEDs will be capable of delivering more than a hundred lumen per device [3]. Various solutions exist to create white light with LEDs, however, luminaries that involve red, green, blue plus possibly intermediate colors give the most complete, flat spectrum, which is required to give the best perceived color quality of the illumination [4]. Advantages of solid-state lighting (SSL) include the possibility to create luminaires in artistic shapes and sizes, or to combine multiple small light sources into one light source. Combinations of many small LEDs maintain good energy efficiency.

While control of traditional light sources is mostly limited to intensity control of the fixed color (white) light, LED technology has the major advantage of additionally allowing the control over the light color and illumination pattern. Hence, the concept of pure illumination may shift into dynamic lighting atmosphere provisioning. It is recognized that smart, intuitive control of a lighting system containing many LEDs, and consequently many parameters to control, is essential for a successful market entry. Figure 1 depicts an intelligent lighting control system that enables such intuitive control. The technology presented in this paper is believed to enable new easy-to-use concepts for control of a large number of LEDs in a lighting environment. This technology is based on uniquely tagging of the light emitted by different LEDs through modulation (via "light link c" in Fig. 1) and a sensor receiving the tags embedded by the LEDs and estimating the light intensity of each LED. In an intelligent lighting system, these estimates would be, together with user input on required lighting pattern, transmitted to a master controller (via "control link a") connected to all the LED lamps (via "control link b").

Modulation of LEDs has been studied in several previous works, though initially mainly for infrared (IR) wireless communications [5]–[8]. Recently, code division multiple access (CDMA) for multiple access for IR communications has been treated in [9]. Currently one can observe an increased interest in visible light communications using powerful lighting LEDs [10]–[13]. The main focus of these papers is on achieving high-speed data communications with arrays of visible light sources. To this end, techniques incompatible with the commonly applied pulse width
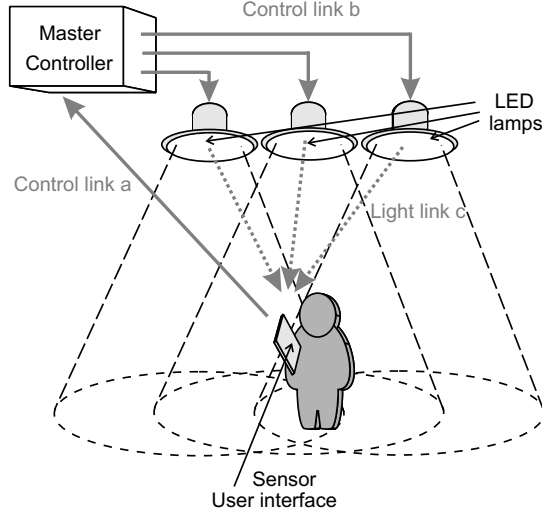
Fig. 1. An illustration of an intelligent lighting control system using coded light.

modulation (PWM) light dimming technique are being proposed, such as orthogonal frequency division multiplexing and discrete multi-tone. Moreover, these works propose to modulate a common data signal on all LEDs in a system/array. Consequently, these techniques are not directly applicable for the local sensing of illumination contributions as considered in this paper. The main performance indicators of our control of the system are, as further detailed in Section II-C, that all light sources can be distinguished individually within the aggregate illumination, that their individual contributions can be estimated regularly, accurately and simultaneously, and that the driving technique of the LEDs is compatible with PWM dimming. However, in our case, aggregate data throughput and bit-error rate (BER) are of little or no relevance.

Therefore, we propose and compare a few possible modulation and multiple-access schemes, along with their multi-signal receiver processing algorithms. First we will introduce CDMA-PPM: a form of pulse-position modulation (PPM) which is keyed according to a spreading sequence, and in which the duty cycle is subject to PWM according to the required dimming levels. To our knowledge our current paper is the first in specifically addressing CDMA *coded light* for the application of lighting control, simultaneously addressing the light source identification and lighting constraints, e.g. estimation accuracy and dimming level, respectively. Moreover, what we proposed also differs from the modulation method proposed as PPM-CDMA in [14], which time-shifts an entire pre-defined CDMA code sequence according to the user data bits. In contrast

to PPM-CDMA, in our CDMA-PPM scheme, the exclusive OR of the user data and the code sequence determines the individual position of each pulse within a series. As a consequence, our waveforms for representing the user bit "0" and "1" are not a time-shifted version of each other, as in [14].

Another scheme is proposed in this work as CDMA-PWM, which is similar to CDMA-PPM, except that we modulate only the start position of the light pulse, but not the end position. Additionally, we allow LEDs not only to be distinguish based on their code but also by their time offset, hence we exploit a hybrid code-time division multiple access (CTDMA). To obtain a pronounceable acronym for CTDMA-PWM and CTDMA-PPM, we nicknamed the system LED-NET.

The main contributions of this paper are:

- The formulation of lighting control via coded light as a research problem, and the formulation of the associated requirements.
- The proposal of a system concept to enable localized lighting control.
- Proposal of two modulation and multiple access schemes, i.e. CDMA-PPM and CTDMA-PWM, and the corresponding multi-signal receiver processing, that enable the proposed system concept.
- A theoretical and numerical performance analysis of the proposed system, not only in terms of real-time measurements of the lighting channel propagation properties, but also in terms of perceivable color error in illumination rendering.

This paper is organized as follows. First, Section II introduces the interaction concepts, system architecture and corresponding system requirements considered in this paper. Section III, subsequently, formulates the LED-NET encoding system and Section IV describes the channel model. In Section V a receiver structure is introduced and its Red-Green-Blue channel estimation performance is studied analytically. In Section VI, this is extended towards the accuracy in color point estimation, which is relevant to quantify the user experience of our control system. Finally, Section VII concludes this paper.

II. Intelligent Lighting Control System

In this section, we introduce the basics of an intelligent lighting control system. We consider a few interaction concepts, present the lighting control system architecture and detail the system

requirements for the modulation and multiple access scheme.

A. Interaction Concepts

Today's concepts of controlling lighting systems are based on wall-mounted switches and remote controls for which a button sequence always affects the same luminary, regardless of where the remote control is being operated. One possible new interaction model for lighting systems is that the user holds a remote control at the location where he wants to control the illumination settings. He presses the control buttons to set the light effect at that particular location. The lighting system then automatically figures out the light contributions of the luminaries that are responsible for the illumination at that location and modifies the light settings of the appropriate luminaries to reach the desired effect. To this end, this paper proposes a modulation method in which the light contributions emitted by all luminaries carry a unique identifying code, which is invisible to the human eye. A sensor in the remote control detects these identifiers for each individual light contribution, identifies (the addresses of) the luminaries involved, and measures the strength of each contribution at the sensor location. This allows the remote control to send a control message to modify the relevant light settings. Moreover, it can measure the resulting changes in a closed control loop.

Another interaction concept can be that the user operates a wall mounted touch display to create specific light effects for predefined locations in the room. Such system requires an initial configuration phase during which a relation is established between desired light parameters and the network addresses of the relevant luminaries. In an environment with thousands of light sources, this commissioning, i.e., the process of assigning the relation between luminaries and their control unit(s), can be cumbersome. In the past, commissioning after the delivery of a large building construction involved the appropriate wiring of power supply cables between individual luminaries and wall switches. This accounted for a significant portion of the total installation costs.

Modern lighting systems increasingly use microcontrollers to switch, dim and control the light sources, and communicate via standards such as Digital Addressable Lighting Interface (DALI), Digital Multiplexing (DMX) or ZigBee. Hence, the commissioning operation changes into finding the network addresses of all luminaries. In future this will be further extended into mapping lighting atmosphere scripts to physical luminaries. Such scripts can for instance use

the physical markup language (PML [15]), a derivative of eXtensible Markup Language (XML), to provide an abstracted description of physical environments and the objects within them, their relationships to the user, to each other and to the space or room. Within a space, all devices, e.g. luminaries controlled by the PML language, collectively act as a browser. Together they render the desired light experience. Each device contains a component that interprets the PML related to the device's capabilities.

Our paper contributes to the realization of such a scenario by proposing a practical, convenient and efficient approach for the discovery of roles and addresses of luminaries, namely by embedding an electronically detectable identification code into each light contribution. A configuration or (re)commissioning operation would then only require a user to hold a remote control once in meaningful locations, relevant to the PML environment.

B. Control System Architecture

Figure 1 schematically describes the considered lighting control system. A control loop is formed by a one-directional light-wave link ("light link c" in Fig. 1) from one or multiple luminaries to a sensor, e.g. placed in a remote control, followed by a link from the sensor to a room controller ("control link a" in Fig. 1), and another link from the room controller to the luminaries ("control link b" in Fig. 1). The focus of this paper is on the first (multiple-access) link, which coincides with the illumination propagation path. The second link can for instance be a ZigBee radio link, or an infrared (IR) link. The third link can be a radio (broadcast) network, a ZigBee network, a wired DALI or DMX network, or involve power line communications. Since the second and third link can be bi-directional, status information from the luminaries such as their temperature, and the associated color spectrum of the emitted light can be shared within the control loop. Alternatively, this information could also be transmitted over the light link. In this paper, however, we only focus on the use of the light link to enable the estimation of the local illumination contributions.

C. System Requirements

We now give a brief account of the requirements posed on the modulation and multiple access schemes for the light link and the corresponding estimation algorithms, such that these are compatible with the popular PWM method of controlling the intensity and color point of LED

lighting. In this PWM method the LEDs are rapidly switched on and off with an appropriate duty cycle. A lower on-period results in a lower average light output level of the LED and, hence, corresponds to a lower dimming level. Changes in color can be achieved by independently changing the dimming levels of co-located LEDs with different colors.

The requirements are listed in order of importance.

a) *Independent illumination and light source identification*: Since the main application of the considered system is illumination, our modulation scheme should not affect the (time-average) duty cycle of any LED. The dimming level must be treated as an external parameter, which needs to be varied per luminary in accordance with the illumination specification to render the desired lighting atmosphere. This may include slow time variations for the generation of effect lighting and independent dimming level settings from one LED to another.

b) *Dimming range*: To enable accurate atmosphere and light color rendering, the modulation method should allow a dimming range of at least 8 bits, but preferably 10 to 12 bits, hence allow a contrast ratio of 1:256 to 1:4096.

c) *Imperceivable*: The modulation scheme and the light dimming method should not cause visible flickering. We believe that, due to the large illuminated area, the requirements are more stringent than for displays, where refresh rates of 50 or 100 Hz are acceptable. In some situations, particularly during rapid eye movements, a human eye can notice frequency components as high as hundreds of Hertz in the illumination [16]. This can be avoided by elimination of low frequency components in the modulation.

d) *Accuracy*: The system must allow measurements of the illumination intensity and color point of the light at distances where the light contributes to the illumination, distinguishing just-noticeable differences defined in human perception models [17], [18].

e) *Simultaneous estimation*: The system must be able to measure the contribution from each locally relevant light source individually and simultaneously. It must operate in an environment with several thousands of LEDs, and be robust against mutual interference.

f) *Complexity*: A (multi-signal) detector must remain simple and low power, to be suited for use in a remote control device.

g) *Interoperable* Our scheme must be usable either with a multi-color light sensor or just with a monochromatic sensor. Moreover, groups of LEDs, e.g. belonging to the same

luminaire, may carry the same identifier, or one may assign a separate identifier for each LED (color component).

h) *Energy efficient*: The tolerable frequency of switching on-off the power of any LED is limited. Power switching causes capacitive losses in the device and its driver circuitry. To maintain a high power efficiency of the luminary, the number of pulses per unit of time needs to be low (say below 1 kHz). We nonetheless will propose to use a high clock frequency for a fine resolution in the pulse position, but to design the illumination pulses to cover a large number of clock cycles without transitions. Moreover, too frequent switching, e.g. if the transients cover more than a few percent of a typical pulse duration, can cause color shifting. During transients, the LED junction is powered differently and typically emits a different spectrum [19], which may create undesirable color artifacts.

i) *Robust*: Ambient light, including sunlight or incandescent and fluorescent lighting should not harmfully impair reliable detection of the modulation scheme. However, our system is less vulnerable to notorious excessive shot noise that high-speed communication would experience in very bright ambient light. In our system, a LED light source needs only to be accurately measurable if its light output power contributes significantly to the local perceived illumination.

j) *Rapid estimation*: The modulation method should allow fast channel estimation. This guarantees that the user experiences an immediate reaction after pressing a control button. Hence, a sensor should be able to identify and measure all relevant light sources within several tenths of a second.

In the remainder of this paper, we will challenge our choices for the modulation system and its parameters against these requirements, and in particular quantify the performance with regard to requirement d).

III. MODULATION AND MULTIPLE ACCESS

In this section, we propose the CTDMA-PPM and CTDMA-PWM visible light modulation schemes, which are designed to embed identifiers in the light, while meeting the requirements posed in Section II-C. We introduce a three-layer structure for the LED-NET modulation and use the following nomenclature for modulated pulses:

- A *slot* has duration T_1. It represents the clock timing at which the power LEDs are driven. Hence T_1 is the resolution at which the LEDs can be modulated.

- A *block* has duration $T_2 = N_1 T_1$ and represents the duration of one chip. The ratio $1 : N_1$ is the contrast ratio and also the resolution of the possible adjustment of the duty cycle for dimming purposes. This corresponds to $q = \log_2 N_1$ bits in dimming capabilities. In one block duration, an LED emits one pulse. The unique property of this modulation method is that the pulse could extend beyond the boundary of the block, according to the illumination requirements.

- A *frame* has duration $T_3 = N_2 T_2$ and it is the time interval during which an identifier is transmitted, and one measurement of the illumination intensity of each LED is made. Hence, when T_3 is in the order of a tenth of a second, requirement j) is satisfied.

As can be understood from the signal description in the next sections, our timing scheme attempts to satisfy requirements b) and a), in blocks and frames, respectively.

A. Block modulation format

Here we introduce binary PPM and PWM for a pulse of amplitude A_l and timing reference τ_l with $\tau_l \in \{0, 1, \ldots, N_1 - 1\}$. These are illustrated in Fig. 2.
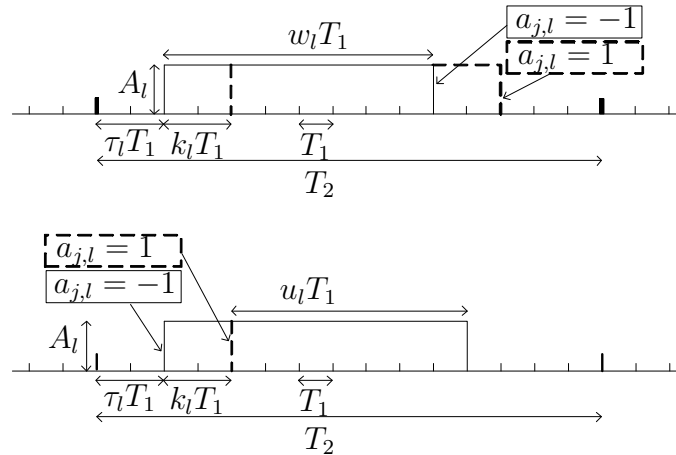

Fig. 2. Description of the binary modulation formats. Pulse position modulation (top) and pulse width modulation (bottom).

1) Pulse position data modulation (PPM)

For PPM, as illustrated in the top part of Fig. 2:

- The starting position of the jth pulse for the lth LED, with $j = 0, \ldots, N_2 - 1$ and $l = 1, \ldots, L$, is given by

$$\delta_{j,l} = \begin{cases} \tau_l, & a_{j,l} = -1 \\ \tau_l + k_l, & a_{j,l} = 1 \end{cases} \tag{1}$$

where τ_l and k_l are the allocated time slot and the modulation depth for the lth LED, respectively, and $a_{j,l}$ denotes the jth chip of the spreading sequence or identification code for the lth LED, where $a_{j,l} \in \{+1, -1\}$. The length of the spreading sequence is N_2.

- The pulse width in terms of number of slots is given by

$$w_l = \text{round}(p_l N_1), \tag{2}$$

where $\text{round}(\cdot)$ rounds to the nearest integer and $(1 - p_l)$ is the dimming level of the lth LED, with $0 \leq p_l \leq 1$. Note that the dimming level is a parameter that can be varied per LED.

2) Pulse width data modulation (PWM)

For PWM, as illustrated in the lower part of Fig. 2:

- The starting position of the jth pulse for the lth LED is the same as used for PPM, i.e., it is given given by $\delta_{j,l}$ as defined in (1).

- The pulse width, however, depends not only on the required light level but, to a small extent, also on the spreading chip, i.e.

$$w_{j,l} = \begin{cases} u_l, & a_{j,l} = 1 \\ u_l + k_l, & a_{j,l} = -1 \end{cases}, \tag{3}$$

where $u_l = \text{round}(p_l N_1 - k_l/2)$. Consequently, pulses end at $\{\tau_l + u_l + k_l\} \bmod N_1$ regardless of $a_{j,l}$. To satisfy the required duty cycle exactly over the frame interval T_3 and meet requirement a), we balance the number of 1's and -1's in the identification/spreading code, i.e., $\sum_{j=1}^{N_2} a_{j,l} = 0$.

Evidently, if we need to transfer any identification code, we cannot switch off the light completely. In PPM, light is emitted in at least one slot, so the realized duty cycle $\tilde{p}_l \geq 1/N_1$. Similarly for PWM, $\tilde{p}_l \geq 1/(2N_1)$ for a balanced number of 1's and -1's in the code. If the total light level in a room must be dimmable to non-perceivable illumination levels this might present a problem. On the other hand, the minimum light level can be made arbitrarily small by

choosing appropriate T_1 and A_l. Meanwhile, the maximum dimming level also needs to remain slightly below 100%, viz. $\tilde{p}_l \leq (N_1 - 1)/N_1$ and $\tilde{p}_l \leq (2N_1 - 1)/2N_1$ for PPM and PWM, respectively. This does not lead to any practical limitation because it has only a minor impact (fractions of a percent) on the lighting intensity given by an LED.

B. Framing

We consider a synchronous system in which T_1, N_1 and N_2 are identical for all LEDs, and their slots, blocks and frames are aligned. We will omit the notational details of pulses extending into neighboring blocks, and we only consider the first frame in a continuous sequence of frames. The signal driving the lth LED can be expressed as

$$s_l(t) = \sum_{j=0}^{N_2-1} \sum_{n=0}^{N_1-1} s_{j,n,l} \Pi \left(\frac{t - jT_2 - nT_1}{T_1} \right).$$ (4)

Here n and j refer to the positions of slots in a block, and to blocks in the frame, respectively, and $\Pi(t) = U(t) - U(t-1)$ is the unit pulse of unit time width and amplitude, where $U(t)$ is the unit step function. The discrete-time signal $s_{j,n,l}$ represents the sample of $s_l(t)$ at $t = jT_2 + nT_1$. For PPM it is given by

$$s_{j,n,l} = A_l \cdot \begin{cases} 0 & n = 0, 1, \ldots, \tau_l - 1, \\ \frac{1 - a_{j,l}}{2} & n = \tau_l, \ldots, \tau_l + k_l - 1, \\ 1 & n = \tau_l + k_l, \ldots, \tau_l + w_l - 1, \\ \frac{1 + a_{j,l}}{2} & n = \tau_l + w_l, \ldots, \tau_l + w_l + k_l - 1, \\ 0 & n = \tau_l + w_l + k_l, \ldots, N_1 - 1, \end{cases}$$ (5)

while for the case of PWM, it is given by

$$s_{j,n,l} = A_l \cdot \begin{cases} 0 & n = 0, 1, \ldots, \tau_l - 1, \\ \frac{1 - a_{j,l}}{2} & n = \tau_l, \ldots, \tau_l + k_l - 1, \\ 1 & n = \tau_l + k_l, \ldots, \tau_l + u_l + k_l - 1, \\ 0 & n = \tau_l + u_l + k_l, \ldots, N_1 - 1, \end{cases}$$ (6)

These pulses can be interpreted to consist of a data-carrying prefix, a main illumination pulse and an inversely data-modulated postfix. For the PWM scheme, the duration of the postfix is reduced to zero.

C. Multiple access

For our scheme, we define a two-dimensional multiple access, namely in the code and time dimension.

We choose CDMA to allow multiple light sources to simultaneously emit PWM-dimmed light, even at high duty cycles and nonetheless transmit unique, seperable codes. We propose to use Walsh-Hadamard (WH) codes, since they can ensure perfect orthogonality and allow for computationally efficient multi-signal receiver algorithms, to address requirements e) and f), respectively. By excluding the first WH code, namely the $\{1, 1, ..., 1\}$ DC word, all codes used have a balanced number of 1's and -1's. This further fixes the frame-average duty cycle and shapes the illumination spectrum to make the data modulation imperceivable, to meet requirements a) and c), respectively. Moreover, the system becomes resilient to sources of constant or sufficiently slowly varying interfering light sources such as sunlight or incandescent bulbs, addressing requirement i). The lth LED is assigned the identification/spreading code

$$\mathbf{a}_{\gamma_l} = [a_{0,\gamma_l}, a_{1,\gamma_l}, \ldots, a_{N_2-1,\gamma_l}]^T, \tag{7}$$

which corresponds to WH code γ_l, with $\gamma_l \in \{2, 3, ..., N_2\}$.

We, additionally, assign a timing reference τ_l to each LED, where each combination (τ_l, γ_l) is unique in the system, i.e., it characterizes one LED. Moreover we avoid that any part of the prefix of postfix of one LED overlaps with the prefix of postfix of another LED that has the same code assigned.

Hence, for CTDMA-PWM, two signals for LED l with (τ_l, γ_l) and LED l' with $(\tau_{l'}, \gamma_{l'})$ and $k_l = k_{l'} = 1$ are orthogonal if $\tau_l \neq \tau_{l'}$ even if $\gamma_l = \gamma_{l'}$. Consequently, the upper bound to the number of orthogonal LEDs equals $N_1 N_2$. CTDMA-PPM has the same upper bound is equal, however, to limit receiver complexity it is more convenient to bound the number of LEDs to $N_1 N_2 / 2$ due to the data carrying pre- and postfix.

For CTDMA-PPM, code and time reference assignment can be challenging because of the arbitrary, luminary-dependent and possibly varying illumination pulse duration. Hence, a pragmatic approach is to let τ_l to be the same for every LED and assign a unique code indexed by γ_l.

The proposed multiple access method allows the sensor to detect multiple signals from LEDs, simultaneously, independent of the different illumination levels, meeting requirements a) and e).

IV. CHANNEL MODEL

As shown in the system block diagram of Fig. 3, the electrical channel is described by the relation of signal $s_l(t)$ output of the lth LED driver, i.e. the transmitter, and signal $y_m(t)$, at the output of the mth sensor, that is offered to the receiver. The corresponding optical transmit and receive signals are denoted in the figure as $\varsigma_l(t)$ and $\chi_m(t)$, respectively. In the following we will consider only one sensor and thus omit the index m.
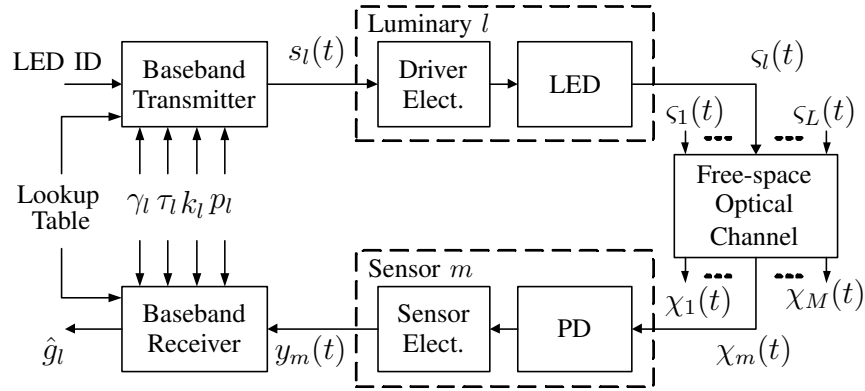

Fig. 3. Block diagram of the link between the lth luminary and mth sensor.

A. Electro-Optical Conversion

The optical transmit signal $\varsigma_l(t)$ in response to a step function of the electrical transmit signal $s_l(t) = A_l U(t)$ is given by $\varsigma_l(t) = A_l \eta_l h_{\mathrm{on}}(t)$ [20], where η_l denotes the LED responsivity. The unit step response of LEDs appears approximately an exponential function [21], i.e.,

$$h_{\mathrm{on}}(t) = U(t)[1 - \exp(-t/\tau_{\mathrm{on}})], \tag{8}$$

$$h_{\mathrm{off}}(t) = 1 - U(t)[1 - \exp(-t/\tau_{\mathrm{off}})]. \tag{9}$$

The time constants τ_{on} and τ_{off} for on- and off-switching tend to differ [22]. These switching effects are considered here, since they are much more pronounced in power and phosphor-coated LEDs than in typical LEDs designed for IR communications. Ignoring a possibly more complicated interaction between the on- and off-tails for very short pulses, the CTDMA-PPM

optical signal becomes

$$\varsigma_l(t) = \sum_{j=0}^{N_2-1} A_l \eta_l h_{\text{on}}\left(t - \delta_{j,l}T_1 - jT_2\right) h_{\text{off}}\left(t - (\delta_{j,l} + w_l)T_1 - jT_2\right). \tag{10}$$

For CTDMA-PWM, $\varsigma_l(t)$ is also given by (10), but now with w_l replaced by $w_{j,l}$ of (3).

B. Indoor Light Propagation

The LED light reaches the sensor possibly via multiple paths, as studied for instance by [5], [6], [23]–[28]. To address requirements b) and j), we will have $T_1 \approx 1$ μs for typical commercial power LEDs. For such a slot time, the inter-symbol interference caused by multipath propagation can be considered negligible. Yet, reflections may change the color content of the light and, as a result, the detector sees different channel amplitudes for differently colored LED light. This is in agreement with requirement d). For the analyses in this paper, however, we model a line-of-sight path as schematically depicted in Fig. 4.
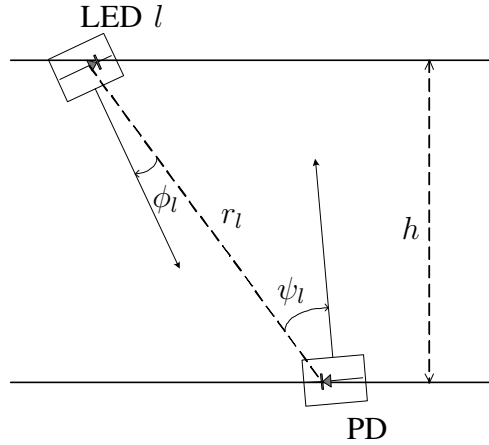

Fig. 4. Geometry of the path between the lth LED and the photodiode (PD).

The gain of such an optical path is

$$\alpha_l = \frac{1}{r_l^2} R(\phi_l) \mathcal{A} \cos(\psi_l), \tag{11}$$

where r_l is the propagation distance, $\mathcal{A}$ is the area of the photodiode (PD) and the angle ψ_l defines the orientation of LED l. Further, $R(\phi_l)$ describes the LED radiation pattern, which we assume to be rotationally symmetric and includes the effects of the lens. The angle ϕ_l defines

the orientation of the PD with respect to the lth LED. We can model $R(\phi_l)$ by a generalized Lambertian law [5], [20]

$$R(\phi_l) = \frac{\mu + 1}{2\pi} \cos^\mu(\phi_l), \tag{12}$$

where μ represents the Lambertian mode number.

C. Opto-Electrical Conversion

The PD in the receiver converts the incoming optical signal into the electrical signal $y(t)$. Its responsivity is denoted by ε_l, which is color dependent and thus carries index l. The speed of PDs is generally much higher than that of power LEDs, hence, switching effects can be considered negligible [20], [29].

D. Channel Disturbances

There are three major sources of channel disturbances, i.e., the background light, the electronics noise and the shot noise.

The background light consists of light contributions from other ambient sources, such as the sun, incandescent and gas discharge lamps. Its power is denoted by $\zeta(t)$. Fluctuations of $\zeta(t)$ that are slower than T_3^{-1} can be approximated as DC during each frame. In the following this is assumed to be valid by design and the argument t is omitted. It is moreover assumed that these background light sources do not result in saturation of the receiver.

Electronics noise is mostly created by the transimpedance amplifier for the PD signal, and predominantly behaves as additive Gaussian (thermal) noise. For a power spectral density (PSD) S_{th} [A^2/Hz] in an effective bandwidth B_{n}, the variance of the thermal noise equals

$$\sigma_{\text{th}}^2 = S_{\text{th}} B_{\text{n}}. \tag{13}$$

Shot noise is due to a stream of electrons that are generated at random times in the PD. It is approximately Gaussian distributed due to the central limit theorem [6]. The shot noise power σ_{shot}^2 is linearly proportional to *all* light shed on the PD surface, not only including the light from LEDs, but also the background light. Hence it can be expressed as

$$\sigma_{\text{shot}}^2(t) = 2q_{\text{e}} B_{\text{n}} \left(\sum_{l=1}^{L} \alpha_l \varepsilon_l \varsigma_l(t) + \varepsilon_\zeta \zeta \right), \tag{14}$$

where q_e is the electrical charge of an electron ($q_e = 1.6 \cdot 10^{-19}$ Coulomb), L denotes the total number of LEDs and ε_ζ is the PD responsivity to background light. Due to the definition of the LED signals $s_l(t)$ in (4), within a frame the shot noise is approximately cyclostationary with period T_2, i.e., $\sigma_{\text{shot}}^2(t) \approx \sigma_{\text{shot}}^2(t + jT_2) = \sigma_{\text{shot},j}^2(t)$ for $j = 1, \ldots, N_2 - 1$.

Hence, the received electrical signal can be written as

$$y(t) = \sum_{l=1}^{L} \alpha_l \varepsilon_l \varsigma_l(t) + v_\zeta + v_{\text{th}}(t) + v_{\text{shot}}(t), \tag{15}$$

where $v_\zeta = \varepsilon_\zeta \zeta$, $v_{\text{th}}(t)$ and $v_{\text{shot}}(t)$ denote the background light contribution, thermal and shot noise terms, respectively. The variances for the latter two are defined in (13) and (14).

V. RECEIVER DESIGN AND PERFORMANCE ANALYSIS

The baseband receiver processing consists of three main steps. To achieve a low-complexity receiver implementation, we first apply integrate-and-dump (I&D) processing to the received signal to yield a discrete time signal. This is followed by CDMA despreading with the assigned CDMA codes to obtain the despreaded signal values for each τ and code in the second step. In the third step we apply an estimator to find the illumination intensities for the different light sources. In this paper we focus on linear estimators.

The I&D receiver outputs the $N_2 \times N_1$ matrix $\mathbf{Y}$, whose (j, n)th element equals

$$y_{j,n} = \frac{1}{T_1} \int_{t=jT_2+(n-1)T_1}^{t=jT_2+nT_1} y(t)\mathrm{d}t. \tag{16}$$

Hence, $\mathbf{Y}$ captures one entire frame. For CDMA despreading for the lth LED, we use a submatrix of $\mathbf{Y}$, denoted by $\mathbf{Y}_l$, containing the columns with the data measurements related to the lth LED. For CTDMA-PPM these are, by design, the columns $n = \tau_l, \ldots, \tau_l + 2k_l - 1$ and $n = \tau_l + w_l, \ldots, \tau_l + w_l + 2k_l - 1$ of $\mathbf{Y}$, relating to the data carrying pre- and postfix, respectively. For CTDMA-PWM the columns $n = \tau_l, \ldots, \tau_l + 2k_l - 1$ of $\mathbf{Y}$ form $\mathbf{Y}_l$.

The despreaded signal vector $\mathbf{d}_l$ is then found by multiplication of the matrix $\mathbf{Y}_l$ with the code vector $\mathbf{a}_{\gamma_l}$, as defined in (7). The result is given by the vector

$$\mathbf{d}_l = \frac{2}{N_2} \mathbf{Y}_l^T \mathbf{a}_{\gamma_l}, \tag{17}$$

of size $4k_l \times 1$ and $2k_l \times 1$ for CTDMA-PPM and CTDMA-PWM, respectively.

Let us define the individual light intensity from the lth LED at the sensor location to be $g_l = A_l \alpha_l \eta_l$. Moreover, let $\mathbf{d}_{\text{noise}}$ denote a zero-mean Gaussian distributed noise vector, modelling

both the thermal and shot noises. The variance of the pth element equals $\sigma_p^2 = 4(\sigma_{\text{th}}^2 + \sigma_{\text{shot},p}^2)/N_2$. Also, let us define the vector $\mathbf{h}_l$, which, if τ_{on} and τ_{off} are small with respect to w_l and with respect to k_l, equals $[\mathbf{h}_{l,\text{on}}, \mathbf{h}_{l,\text{off}}]$ and $\mathbf{h}_{l,\text{on}}$ for CTDMA-PPM and CTDMA-PWM, respectively. Here the $2k_l \times 1$ vectors $\mathbf{h}_{l,\text{on}}$ and $\mathbf{h}_{l,\text{off}}$ are given by

$$\mathbf{h}_{l,\text{on}} = \varepsilon_l [h_{\text{on},1}, \cdots, h_{\text{on},k_l}, h_{\text{on},k_l+1} - h_{\text{on},1}, \cdots, h_{\text{on},2k_l} - h_{\text{on},k_l}]^T, \tag{18}$$

$$\mathbf{h}_{l,\text{off}} = \varepsilon_l [h_{\text{off},1}, \cdots, h_{\text{off},k_l}, h_{\text{off},k_l+1} - h_{\text{off},1}, \cdots, h_{\text{off},2k_l} - h_{\text{off},k_l}]^T, \tag{19}$$

respectively. Due to the I&D receiver structure in (16) and the channel behavior in (8) and (9), the elements of $\mathbf{h}_{l,\text{on}}$ and $\mathbf{h}_{l,\text{off}}$ are given by

$$\begin{aligned}
h_{\text{on},i} &= \frac{1}{T_1} \int_{(i-1)T_1}^{iT_1} [1 - \exp(-t/\tau_{\text{on}})] \, \mathrm{d}t \\
&= 1 - \frac{\tau_{\text{on}}}{T_1} [\exp(-(i-1)T_1/\tau_{\text{on}}) - \exp(-iT_1/\tau_{\text{on}})],
\end{aligned} \tag{20}$$

and similarly

$$h_{\text{off},i} = 1 - \frac{\tau_{\text{off}}}{T_1} [\exp(-(i-1)T_1/\tau_{\text{off}}) - \exp(-iT_1/\tau_{\text{off}})]. \tag{21}$$

Using these definitions we can rewrite the despreaded signal vector, as defined in (17), to

$$\mathbf{d}_l = \frac{2}{N_2} \mathbf{Y}_l^T \mathbf{a}_{\gamma_l} = g_l b_l \mathbf{h}_l + \mathbf{d}_{\text{noise}}. \tag{22}$$

Note that it is reasonable to assume $\mathbf{h}_l$ is known by the receiver.

It is noted that in (22) the interference between LEDs is zero, since orthogonal codes are assigned to the LEDs applying the same slots for data modulation. Requirement e) is thus satisfied. Moreover, the illumination pulses and background light v_ζ can be considered as modulated light applying the WH-code with $\gamma_l = 1$, i.e., the DC code, which is orthogonal to all codes applied in the pre- and postfixes. Hence, the illumination pulses and background light are perfectly removed by the despreading of (17). Hence, requirement i) is satisfied.

Moreover, we can use this to make an estimate of the shot noise variance σ_{shot}^2, which can be used to design bit detection and intensity estimation algorithms in the following sections. For that we correlate the received signal matrix for the lth LED $\mathbf{Y}_l$ with the DC code, yielding a vector containing the sum of the background light and illumination pulses, denoted by $\mathbf{d}_{l,\text{DC}}$. Using (14) this can be related to the shot noise variance.

A. Intensity Estimation

It was explained in Section II that it is essential to measure the individual light level g_l in an intelligent light system. A linear estimator of g_l can be written as a multiplication of the despreaded vector $\mathbf{d}_l$ with the weighting vector $\boldsymbol{\xi}_l$ of size $2k_l \times 1$ and $4k_l \times 1$ for CTDMA-PWM and CTDMA-PPM, respectively. The result is given by

$$\hat{g}_l = \boldsymbol{\xi}_l^T \mathbf{d}_l. \tag{23}$$

One can choose the weight vector $\boldsymbol{\xi}_l$ according to the least squares (LS) and the minimum mean square error (MMSE) criteria, which reflect the cases that the variance of $\mathbf{d}_{\text{noise}}$ is unknown and known, respectively.

1) LS Estimation: For LS estimation of g_l, the weight vector becomes

$$\boldsymbol{\xi}_{l,\text{LS}} = (\mathbf{h}_l^T \mathbf{h}_l)^{-1} \mathbf{h}_l. \tag{24}$$

For the special case in which power LEDs are switched on and off instantaneously, i.e., $\tau_{\text{on}}, \tau_{\text{off}} \ll T_1$, and that the elements of $\mathbf{d}_{\text{noise}}$ are i.i.d., $\boldsymbol{\xi}_l$ can be chosen according to equal gain combining. Hence, the pth element of $\boldsymbol{\xi}_l$, denoted by $\xi_{l,p}$, equals 1 for $0 \le p \le k_l - 1$ (for both CTDMA-PPM and CTDMA-PWM) and for $2k_l \le p \le 3k_l - 1$ (for CTDMA-PPM) and $\xi_{l,p} = 0$, otherwise.

For performance analysis, we use

$$\hat{g}_{l,\text{LS}} = g_l + (\mathbf{h}_l^T \mathbf{h}_l)^{-1} \mathbf{h}_l^T \mathbf{d}_{\text{noise}}. \tag{25}$$

The second term is the least square error (LSE), which is a zero-mean random Gaussian variable with mean squared value

$$\sigma_{\text{LSE},l}^2 = (\mathbf{h}_l^T \mathbf{h}_l)^{-2} \mathbf{h}_l^T \mathbf{R}_{\text{noise}} \mathbf{h}_l, \tag{26}$$

where $\mathbf{R}_{\text{noise}} = \mathbb{E}[\mathbf{d}_{\text{noise}} \mathbf{d}_{\text{noise}}^T]$ and $\mathbb{E}$ denotes expectation. If the noise is i.i.d, i.e. $\mathbf{R}_{\text{noise}} = \sigma^2 \mathbf{I}$, where $\mathbf{I}$ is the identity matrix, then

$$\sigma_{\text{LSE},l}^2 = \frac{\sigma^2}{\|\mathbf{h}_l\|^2} = \frac{4(\sigma_{\text{th}}^2 + \sigma_{\text{shot}}^2)}{N_2 \|\mathbf{h}_l\|^2}, \tag{27}$$

where $\|\cdot\|$ denotes the Euclidean norm. For this scenario we can calculate the lower bound on the mean squared LSE. It can be easily shown that this is achieved when $\tau_{\text{on}} = \tau_{\text{off}} = 0$ and is

given by

$$\sigma^2_{\text{LSE},l,\text{PPM}} \geq \frac{2(\sigma^2_{\text{th}} + \sigma^2_{\text{shot}})}{k_l N_2 \varepsilon^2_l}, \tag{28}$$

$$\sigma^2_{\text{LSE},l,\text{PWM}} \geq \frac{4(\sigma^2_{\text{th}} + \sigma^2_{\text{shot}})}{k_l N_2 \varepsilon^2_l}, \tag{29}$$

for CTDMA-PPM and CTDMA-PWM, respectively.

It can be observed that the LSE is a factor 2 smaller for CTDMA-PPM than for CTDMA-PWM. The LS estimation process suffers from a reduction of SNR due to the non-ideal response of the LEDs, i.e., the LSE will increase with increasing τ_{on} and τ_{off}. Moreover, an increase in code length N_2 and modulation depth k_l increases the MSE performance.

2) Linear MMSE Estimation: The LS intensity estimator is unbiased, but it suffers from noise enhancement. Therefore we explore the use of the MMSE estimator. MMSE estimation for known $\mathbf{R}_{\text{noise}}$ can be realized by estimating the variance of the shot noise through the DC-code contribution, as explained at the beginning of this section.

The MMSE estimator is found as the estimator that minimizes the cost function

$$\begin{aligned} \sigma^2_{l,\text{MMSE}} &= \mathbb{E}\left[(\hat{g}_l - g_l)^2\right] = \mathbb{E}\left[\left(\boldsymbol{\xi}^T_l \mathbf{d}_l - g_l\right)^2\right] \\ &= g^2_l - 2\mathbb{E}\left[g_i \boldsymbol{\xi}^T_l \mathbf{d}_l\right] + \mathbb{E}\left[\boldsymbol{\xi}^T_l \mathbf{d}_l \mathbf{d}^T_l \boldsymbol{\xi}_l\right]. \end{aligned} \tag{30}$$

Consequently, the MMSE estimator can be shown to be given by

$$\boldsymbol{\xi}_{l,\text{MMSE}} = \left(1/\mathbb{E}[g^2_l] + \mathbf{h}^T_l \mathbf{R}^{-1}_{\text{noise}} \mathbf{h}_l\right)^{-1} \mathbf{R}^{-1}_{\text{noise}} \mathbf{h}_l, \tag{31}$$

and the resulting mean squared estimation error equals

$$\sigma^2_{\text{MMSE},l} = (1/\mathbb{E}[g^2_l] + \mathbf{h}^T_l \mathbf{R}^{-1}_{\text{noise}} \mathbf{h}_l)^{-1}. \tag{32}$$

For i.i.d. noise, $\sigma^2_{\text{MMSE},l}$ is given by

$$\sigma^2_{\text{MMSE},l} = \frac{\sigma^2}{\frac{\sigma^2}{\mathbb{E}[g^2_l]} + \|\mathbf{h}_l\|^2} = \frac{(\sigma^2_{\text{th}} + \sigma^2_{\text{shot}})}{\frac{(\sigma^2_{\text{th}} + \sigma^2_{\text{shot}})}{\mathbb{E}[g^2_l]} + \frac{N_2 \|\mathbf{h}_l\|^2}{4}}. \tag{33}$$

Similarly as for the LS estimator, the lower bound of $\sigma^2_{\text{MMSE},l}$ can be obtained as

$$\sigma^2_{\text{MMSE},l,\text{PPM}} \geq \frac{\sigma^2_{\text{th}} + \sigma^2_{\text{shot}}}{\frac{\sigma^2_{\text{th}} + \sigma^2_{\text{shot}}}{\mathbb{E}[g^2_l]} + \frac{k_l N_2 \varepsilon^2_l}{2}}, \tag{34}$$

$$\sigma^2_{\text{MMSE},l,\text{PWM}} \geq \frac{\sigma^2_{\text{th}} + \sigma^2_{\text{shot}}}{\frac{\sigma^2_{\text{th}} + \sigma^2_{\text{shot}}}{\mathbb{E}[g^2_l]} + \frac{k_l N_2 \varepsilon^2_l}{4}}, \tag{35}$$

for CTDMA-PPM and CTDMA-PWM, respectively.

It can be observed from (28), (29), (34) and (35) that when the SNR is high, the MMSE estimator and LS estimator tend to become equivalent. The performance difference between CTDMA-PPM and CTDMA-PWM is similar as for the LS estimator.

Numerical results for the intensity estimation performance will be given in Section VI-A.

B. Complexity Evaluation

In this subsection we evaluate the computational complexity required in the receiver and intensity estimation.

In every frame period, i.e. T_3, the receiver writes $N_1 N_2$ samples to its memory to form $\mathbf{Y}$. It is then most efficient to implement the correlation processing of (17) for all LEDs simultaneously. This is done by applying N_1 WH transforms to $\mathbf{Y}$. Each transform involves $N_2 \log(N_2)$ real additions.

Let N_c denote the number of samples combined for each intensity estimation in (23). Hence, N_c equals the number of non-zero elements in $\boldsymbol{\xi}_l$, which for PWM is smaller than $2k_l$ and for PPM is smaller than $4k_l$. Each LS intensity estimation requires N_c multiplications, $N_c - 1$ additions and one abs($\cdot$) operation. Each MMSE intensity estimation, requires, however, inverting a $N_c \times N_c$ matrix, in addition to the computations needed for LS intensity estimation.

Let us consider a basic implementation using $k_l = 1 \ \forall l$ and CTDMA-PWM, where the switching speed of LEDs are very high, i.e. $\tau_{\text{on}} \ll T_1$ and $\tau_{\text{off}} \ll T_1$. Each LS intensity estimate requires one abs($\cdot$) operation and each MMSE estimation requires one addition, one division and one abs($\cdot$) operation. Hence, the complexity of such detector is low, addressing requirement f).

This simple receiver can make one measurement of the light intensity from $(N_2 - 1)$ encoded LED signals for each time division bin. There are N_1 possible starting positions τ_l, but bins have width k_l. Hence the number of estimates per slot of length T_1 becomes

$$S_1 = \frac{(N_2 - 1)N_1}{k} \frac{1}{N_1 N_2} = \frac{(N_2 - 1)}{N_2} \frac{1}{k} \ \ [\text{bits}]. \tag{36}$$

For large N_2 and $k = 1$ this tends to unity. Hence the system can make close to one LED intensity measurement per T_1. We believe that thereby we reach a fundamental limit for binary (on-off) modulation. Meanwhile, the schemes allow an arbitrary dimming of each LED independently, at a resolution of $2^q = N_1$ steps to meet requirement b). Although the LEDs are clocked at a rate

of T_1^{-1}, in each block, i.e. T_2, only a single power-on and power-off transition is made. This limits the capacitive losses to address requirement h).

VI. NUMERICAL RESULTS

In this section, we present the numerical results calculated based on a scenario for a large indoor environment of 40 m $\times$ 40 m with a high density of LEDs. In this scenario, the illumination LEDs are distributed in a square grid with a dimension of 25 cm, i.e., a density of 16 LED lamps/m^2 that all consist of a co-located red, green and blue LED. Consequently, the full ceiling is covered with a total of 3×25600 LEDs. These lamps generate light with a color temperature of 6500 K (D65) [30] for equal duty cycles of the red, green and blue LEDs, i.e., for $p_r = p_g = p_b$. The sensor is located in the middle of the room and is oriented such that it faces the ceiling at a distance of h = 3.5 m. For the lamp and sensor parameters we consider Philips Lumileds LUXEON K2 LEDs [31] and a Hamamatsu S6468 monochromatic photodetector [32]. The Lambertian mode number μ is the same for all LEDs. The area of the PD $\mathcal{A} = 10^{-4}$ m^2. For the red, green and blue LEDs, the driving currents I are 0.25, 1.1 and 0.22 A, respectively, which corresponds to a lumen output of 43.7, 142 and 9.72. The responsivity of the LEDs η equals 1.30, 0.243 and 0.89 W/A and that of the PD ε equals 0.42, 0.28, 0.21 A/W for the red, green and blue LEDs, respectively.

Walsh-Hadamard codes with $N_2 = 256$ are used, and N_1 is set to be 1024 to provide a dimming range of 10 bits. Every LED takes $k_l = k = 5$ slots for modulation. The slot period $T_1 = 1$ μs and we assume $\tau_{\text{on}} \ll T_1$ and $\tau_{\text{off}} \ll T_1$. In this simulation, all LEDs are considered to operate at the same duty cycle of 50%, i.e., $p_l = 0.5 \; \forall l$. The PSD of electronics noise $S_{\text{th}} = 1.69 \times 10^{-24}$. While all the LEDs are radiating light and embedding codes simultaneously, we consider only the sensing performances of the link between one LED and the sensor.

In this scenario with high LED density, the shot noise is dominated by the light contributions of the LEDs, i.e., the first term in (14). This large room scenario can be considered a worst case scenario, since many LEDs contribute to the shot noise. Inspection of simulation runs confirmed that, due the large number of LEDs that simultaneously emit illumination pulses, the variance of the shot noise (14) becomes stationary and identical for all slots in a frame, with $\sigma_{\text{shot}}^2 = 2q_e B_n P_{\text{light}}$. Here P_{light} is the average light level on the photodetector and is given by $P_{\text{light}} = p_a \mathcal{A} M(\mu)$, where p_a denotes the average duty cycle and $M(\mu)$ equals 4.00, 4.09 and
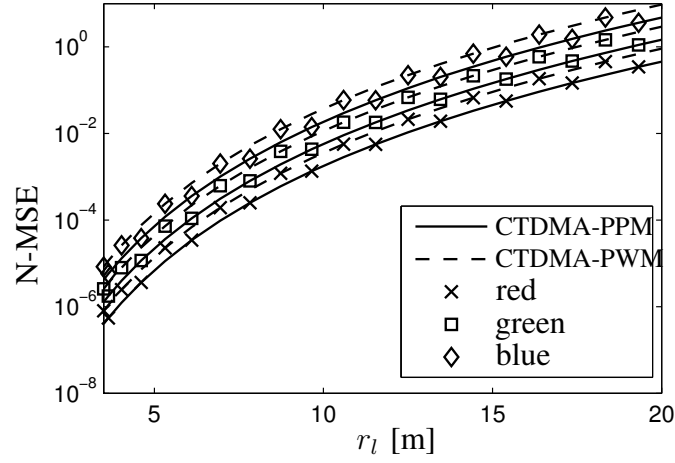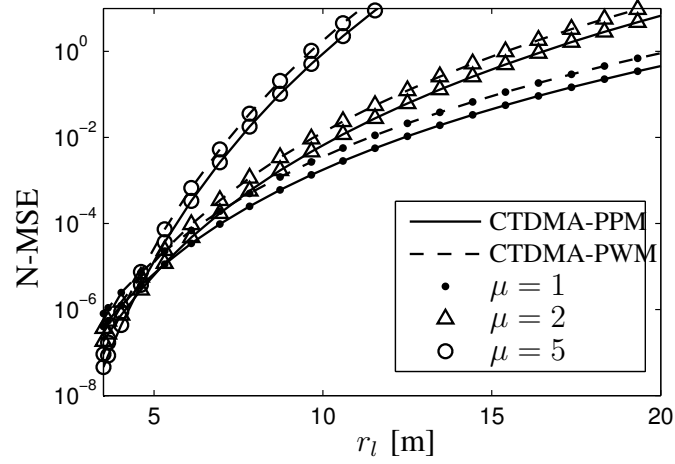
4.10 for the Lambertian mode number μ equals 1, 2, and 3 respectively. For larger values of μ, $M(\mu)$ approximately equals $M(3)$. It is verified that taking LEDs with larger separation into account, i.e., for distances larger than 40 m from the PD, would not significantly increase P_{light}. Consequently, the considered case is a worst case scenario considering the level of generated shot noise due to other light sources.

A. MSE in Intensity Estimation

First we illustrate the MSE performance in LS intensity estimation, as derived analytically in (27), for the large room scenario. To this end we study in Fig. 5 the normalized MSE (N-MSE) in light intensity estimation, i.e., the MSE results derived in Section V-A normalized by the squared value of the actual light intensity. We present the MSE results as a function of r_l, the hypotenuse propagation distance according to $r_l = \sqrt{h^2 + x_l^2 + y_l^2}$ with (x_l, y_l) the ceiling grid coordinates of the luminary with respect to the sensor. The sensor is fixed and we take numerical results for LEDs at different locations on the ceiling.

Figure 5(a) depicts the N-MSE for the three color LEDs with $\mu = 1$. It is observed from the depicted results that the performance in intensity estimation degrades in an exponential fashion as the distance between the LED and sensor increases. We can observe that we get considerable estimation errors, N-MSE $> 10^{-2}$, in the intensity estimation using CTDMA-PPM for LEDs whose distances from the sensor are above 12.5, 10.7 and 9.3 m for red, green and blue LEDs, respectively. Over the considered range the difference in color seems to result in a shift of the MSE curves, which again can be attributed to the difference in optical output power and color dependence of the PD responsivity. For CTDMA-PWM these ranges are approximately 1 m smaller, as expected from the results in (28) and (29). The impact of this error, however, is limited since the contribution to the local illumination from LEDs which are beyond these distances are negligible, since their contributions are more than 20 dB lower than that of the LED with the dominant contribution at the sensing location. The above shows that we can satisfy requirement d) up to considerable ranges.

Similar results for red LEDs with different radiation patterns, for $\mu = 1$, 2 and 5, are depicted in Fig. 5(b). For the CTDMA-PPM scheme, N-MSE values below 10^{-2} are now achieved up to distances of 12.5, 10.5 and 7.6 m for μ equals 1, 2 and 5, respectively. The degradation in range for CTDMA-PWM, compared to CTDMA-PPM, is less than 1 m. In contrast to the difference

(a) different color LEDs, $\mu = 1$

(b) red LEDs, different μ values

Fig. 5.   Normalized MSE in intensity estimation vs. PD-LED hypotenuse propagation distance, for a ceiling height of $h = 3.5$ m.

in color, the difference in LED radiation pattern changes the slope of the MSE curve. For very low distances the performance is slightly improved for high μ, i.e., narrow light beams, while for high distances the MSE is significantly increased for high μ.

B. Accuracy in Light Color Estimation

Instead of calculating BER performance as typically occurs in high-speed communication-oriented papers, in this section we illustrate the performance of the proposed methods to estimate and set the color of the light emitted by the color LED lamps, using a monochromatic sensor. In

this procedure the sensor receiver performs an intensity estimation for every LED. Since it also identifies the LEDs, it can obtain the color of the individual LEDs from the master controller and combine this with the intensity estimates to determine the color of the resulting light. When the system can accurately estimate the color of the resulting light, these estimates are also suitable to locally render colors with a control loop.

To study the performance in estimation of local light, we use Monte Carlo simulations of the light color estimation based on the LS estimates of the intensities of the individual colored LEDs with $\mu = 1$. We refer the interested reader to text books on color theory, e.g. [17], [30], which show that the accuracy in color estimation is best evaluated in the commonly used $u'v'$ uniform chromaticity diagram. This diagram is normalized to the sensitivity of the human eye, such that the threshold value for a noticeable color difference is independent of the $u'v'$ color point of the light. For a standard observer, a color difference is only noticeable if the error in the $u'v'$ color diagram, i.e., $\Delta u'v'$, is larger than 0.001 [4], [17], [33].

Figure 6(a) depicts the $u'v'$ points of the primary colors of the LEDs (red, green and blue) and that of 4 mixed colors. The mixed colors are set by varying the duty cycles for the different color LEDs. For the colors white (D65), pink, light green and purple, the ratios between the duty cycles of the red, green and blue LEDs are given by 1:1:1, 1:0.2:0.2, 0.2:1:0.2 and 0.2:0.2:1, respectively. All lamps contribute the same color.

We transformed [17], [30] the simulated estimates (23) into estimated coordinates $\hat{u}'$ and $\hat{v}'$ of u' and v', respectively. The mean of $\Delta u'v'$ is then given $\mathbb{E}\{\Delta u'v'\} = \mathbb{E}\{\sqrt{(\hat{v}' - v')^2 + (\hat{u}' - u')^2}\}$. This mean is plotted in Fig. 6(b) as a function of the perpendicular distance to the ceiling h for the four mixed colors. We conclude from Fig. 6(b) that inside the simulated room for all four rendered colors the mean of $\Delta u'v'$ stays well below the threshold of noticeable color difference. Also we observe a slight difference in color estimation performance for the different color points. This can be explained by the color dependence of the MSE in intensity estimation, as observed in Fig. 5(a). Furthermore, the dependence on height can be attributed to the location and height dependence of the MSE, where it is noted that the performance is quite stable except for sensor locations near the ceiling, in between lamps. This can be explained by the rapidly decreasing signal contributions at these height due to the downward radiation pattern of the LEDs.

The accurate estimation of the color point of the purple light appears to be the most challenging, which corresponds with the fact that the MSE in intensity estimation is highest for the blue

(a) LED and mixed color in $u'v'$ diagram.

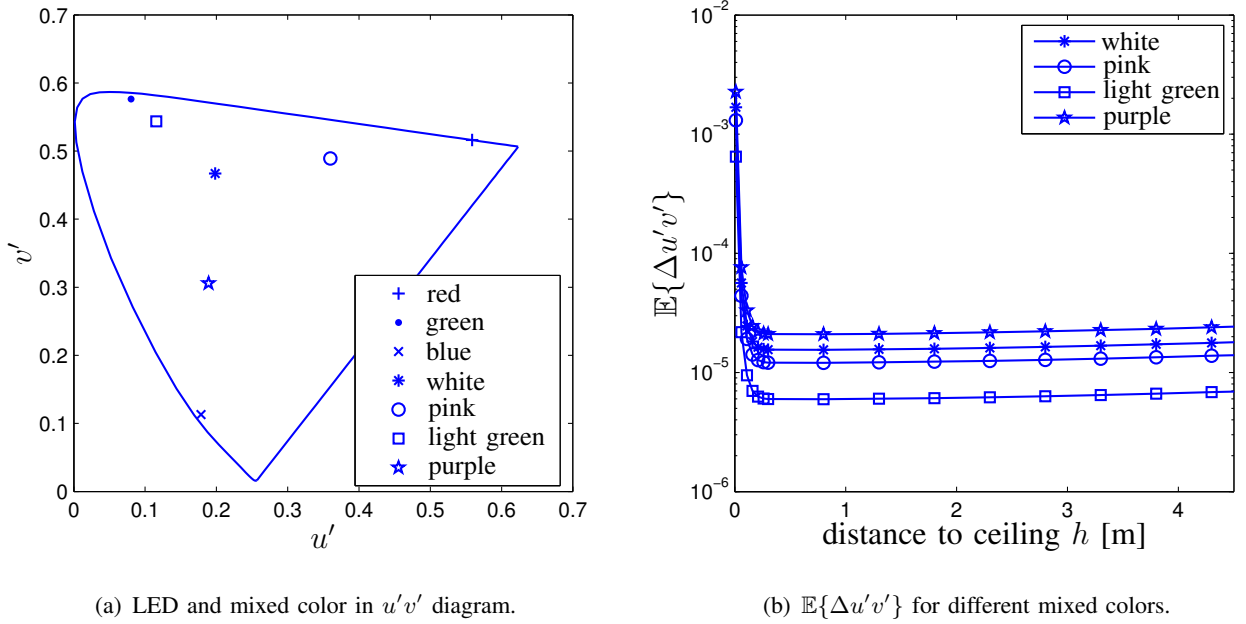(b) $\mathbb{E}\{\Delta u'v'\}$ for different mixed colors.

Fig. 6. Accuracy in color estimation for different mixed colors.

LEDs. On the other hand, the color estimation of pink is worse than that of the light green light, although the MSE for the red LEDs is the lowest. This can be attributed to the transformation to the $u'v'$ plane, which takes into account the sensitivity of the human visual perception system, which is less sensitive to differences in green colors. However, the difference in $\Delta u'v'$ between the different colors is very small and well below the visible threshold, satisfying requirement d). So the proposed method more than adequately estimates the color point of the produced light with a monochromatic sensor.

Extensions to the studied system could be made by the use of a multi-color sensor, which would allow for all three color LEDs in one lamp to use the same $\{\tau_l, \gamma_l\}$.

C. Evaluation

For the large room scenario considered in this section, we proposed a dimming resolution of $q = 10$ bits, i.e. $N_1 = 1024$. Furthermore, we applied a system with $N_2 = 256$, $k = 5$ and $T_1 = 1$ μsec. Thus LEDs are switched around 10^3 times per second, which keeps the capacitive power losses due to on- and off-transients negligibly small, addressing requirement h), yet it is fast enough to prevent visible flickering. Each LED can be measured within a 0.26 s period, to

address requirement j), and the system can simultaneously and separately detect the light from more than 250,000 independent light sources, to satisfy requirement e).

For systems with fewer LEDs, one can decrease the measurement time by choosing a smaller code length N_2. A code length of 32, for example, would yield a measurement of the intensities of all LEDs each 33 ms, while still more than 30,000 LEDs can be supported.

VII. DISCUSSIONS AND CONCLUSIONS

Solid-state lighting will play an increasingly important role in general illumination as well as light effect creation. The intuitive control of sophisticated lighting installations is regarded as a key factor for the market acceptance of such systems. This paper introduced a technology named *coded light* that brings such simplicity by enabling new interaction modes for lighting systems. The technology is based on the embedding of identifiers in the light from high brightness LEDs. This allows for identification and estimation of the light contribution of each LED in a localized manner, which is essential to the deployment of the new user interaction modes.

A set of requirements for such systems were formulated in this paper, which significantly differ from those for the usual wireless optical systems studied hitherto. The differences are caused by the fact that the proposed system is used simultaneously for illumination, transmission of identifiers and lighting control. To satisfy these requirements, we introduced a new class of binary modulation methods suitable for PWM-based dimming, simultaneous identification of multiple SSL luminaires, and estimation of their individual local light contributions. These methods involve the use of a main illumination pulse with a data carrying prefix and/or postfix, and are based on PPM and PWM. A hybrid code and time division multiple access scheme is used to separate the signals from the different LEDs, which allows for a large number of light sources to be measured by the system simultaneously.

A receiver design was proposed. For estimation, the least square and minimum mean square error estimators were studied. Furthermore, the performance of the intensity estimators were derived analytically. The results reveal that the CTDMA-PPM scheme is 3 dB more robust to noise than the CTDMA-PWM scheme in MSE performance. This, however, comes at the cost of a more complicated code and time slot assignment for CTDMA-PPM and a smaller number of LEDs that can be allocation. For our application, the range, data throughput and BER appeared to be less critical than performance measures such as the number of light sources per second

that can be measured individually, and the accuracy of color estimation.

For a worst-case scenario with a very large numbers of LEDs in a room, we evaluated numerically the main system performance parameters. Next to the MSE of RGB color components, we calculated the achievable color accuracy in the $u'v'$ color triangle. We concluded from this study that our approach provides the required MSE performance up to a range of about 7 to 10 meters. It was, moreover, concluded that the error in the estimation of the light color is very small and well below the visible threshold, even for this highly demanding scenario.

REFERENCES

[1] J.-P. M. G. Linnartz, L. Feri, H. Yang, S. B. Colak, and T. C. W. Schenk, "Communications and sensing of illumination contributions in a power led lighting system," in *Proc. International Conference on Communications, Beijing, China*, May 2008, pp. 5396–5400.

[2] E. F. Schubert and J. K. Kim, "Solid-state light sources getting smart," *Science*, vol. 308, pp. 1274–1278, May 2005.

[3] D. A. Steigerwald, J. C. Bhat, D. Collins, R. M. Fletcher, M. O. Holcomb, M. J. Ludowis, P. S. Martin, and S. L. Rudaz, "Illumination with solid state lighting technology," *IEEE J. Select. Topics Quantum Electron.*, vol. 8, pp. 310–320, March/April 2002.

[4] S. Muthu, F. J. P. Schuurmans, and M. D. Pashley, "Red, green, and blue LEDs for white light illumination," *IEEE J. Select. Topics Quantum Electron.*, vol. 8, no. 2, pp. 333–338, Mar./Apr. 2002.

[5] F. R. Gfeller and U. Bapst, "Wireless in-house communication via diffuse infrared radiation," *Proc. IEEE*, vol. 67, no. 11, pp. 1474–1486, Nov. 1979.

[6] J. M. Kahn and J. R. Barry, "Wireless infrared communications," *Proc. IEEE*, vol. 85, no. 2, pp. 265–298, Feb. 1997.

[7] R. Otte, L. P. de Jong, and A. H. M. van Roermund, *Low-power Wireless Infrared Communications*. Springer, 1999.

[8] S. Hranilovic, *Wireless Optical Communication Systems*. New York, NY: Springer, 2004.

[9] U. N. Griner and S. Arnon, "Multiuser diffuse indoor wireless infrared communications using equalized synchronous CDMA," *IEEE Trans. Commun.*, vol. 54, pp. 1654–1662, Sept. 2006.

[10] G. Pang, T. Kwan, H. Liu, and C.-H. Chan, "LED wireless," *IEEE Ind. Appl. Mag.*, vol. 8, no. 1, pp. 21–28, Jan./Feb. 2002.

[11] T. Komine and M. Nakagawa, "Fundamental analysis for visible-light communication system using LED lights," *IEEE Trans. Consumer Electron.*, vol. 50, no. 1, pp. 100–107, Feb. 2004.

[12] M. Z. Afgani, H. Haas, H. Elgala, and D. Knipp, "Visible light communication using ofdm," in *Proc. TRIDENTCOM 2006*, March 2003.

[13] J. Grubor, S. C. J. Lee, K.-D. Langer, A. M. J. Koonen, and J. Walewski, "Wireless high-speed data transmission with phosphorescent white-light leds," in *Proc. ECOC 2007*, Sept. 2007.

[14] J. M. H. Elmirghani and R. A. Cryan, "New PPM-CDMA hybrid for indoor diffuse infrared channels," *Electronics Letters*, vol. 30, pp. 1646–1647, September 1994.

[15] Physical markup language (PML). [Online]. Available: http://web.mit.edu/mecheng/pml/

[16] J. E. Farrell, "An analytical method for predicting perceived flicker," *Behaviour and Information Technology*, vol. 5, pp. 349–358, 1986.

[17] G. Wyszecki and W. S. Stiles, *Color science; concepts and methods, quantitative data and formulas*. New York: Wiley, 1967.

[18] P. R. Boyce, *Human Factors in Lighting*, 2nd ed. London: Taylor & Francis, 2003.

[19] W.-H. Lan, "Wavelength shift of gallium nitride light emitting diode with p-down structure," *IEEE Trans. Electron Devices*, vol. 52, pp. 1217–1219, 2005.

[20] D. Wood, *Optoelectronic Semiconductor Devices*. Prentice Hall, 1994, ch. 1,2,3,5,6.

[21] A. Descombes and W. Guggenbuhl, "Investigation of the influence of several diode parameters on the light-delay time in large-area SH-junction LED's," *IEEE Trans. Electron Devices*, vol. ED-25, no. 3, pp. 379–382, Mar. 1978.

[22] A. Descombes and W. Guggenbuhl, "Large signal circuit model for LED's used in optical communication," *IEEE Trans. Electron Devices*, vol. ED-28, no. 4, pp. 395–404, Apr. 1981.

[23] C. R. Lomba, R. T. Valadas, and A. M. de O. Duarte, "Experimental characterisation and modelling of the reflection of infrared signals and indoor surfaces," *IEE Proc.-Optoelectron.*, vol. 145, no. 3, pp. 191–197, Jun. 1998.

[24] V. Jungnickel, V. Pohl, S. Nönnig, and C. V. Helmolt, "A physical model of the wireless infrared communication channel," *IEEE J. Select. Areas Commun.*, vol. 20, no. 3, pp. 631–640, Apr. 2002.

[25] J. B. Carruthers, S. M. Carroll, and P. Kannan, "Propagation modelling for indoor optical wireless communications using fast multi-receiver channel estimation," *IEE Proc.-Optoelectron.*, vol. 150, no. 5, pp. 473–481, Oct. 2003.

[26] Y. A. Alqudah and M. Kavehrad, "MIMO characterization of indoor wireless optical link using a diffuse-transmission configuration," *IEEE Trans. Commun.*, vol. 51, no. 9, pp. 1554–1560, Sep. 2003.

[27] M. R. Pakravan, M. Kavehrad, and H. Hashemi, "Indoor wireless infrared channel characterization by measurements," *IEEE Trans. Veh. Technol.*, vol. 50, no. 4, pp. 1053–1073, Jul. 2001.

[28] O. Gonzalez, S. Rodriguez, R. Perez-Jimenez, B. R. Mendoza, and A. Ayala, "Error analysis of the simulated impulse reponse on indoor wireless optical channels using a Monte Carlo-based ray-tracing algorithm," *IEEE Trans. Commun.*, vol. 53, no. 1, pp. 124–130, Jan. 2005.

[29] A. E. Iverson and D. L. Smith, "Mathematical modeling of photoconductor transient response," *IEEE Trans. Electron Devices*, vol. 34, pp. 2098–2107, Oct. 1987.

[30] R. Hunt, *The Reproduction of Color*, 6th ed. Wiley and Sons, 2004.

[31] Philips Lumileds, "Technical datasheet DS51, power light source LUXEON K2," available from http://www.lumileds.com/, 2007.

[32] Hamamatsu, "Product sheet S6468, high-speed sensor with preamp," available from http://www.hamamatsu.com/, Jan. 2007.

[33] P. Rizzo, A. Bierman, and M. S. Rea, "Color and brightness discrimination of white LEDs," *Solid State Lighting II: Proceedings of SPIE*, vol. 4776, pp. 235–246, 2002.